LASER AUTOGENOUS BRAZING – A NEW METHOD FOR JOINING DISSIMILAR METALS

Paper #602

Gen Satoh, Y. Lawrence Yao

Manufacturing Research Lab, Columbia University
New York, NY, 10027, USA

Abstract

The joining of dissimilar metals is a critical process for the future development and evolution of medical devices which would enable the selective use of the unique properties exhibited by biocompatible materials such as stainless steel and titanium, as well as shape memory materials such as NiTi to locally tailor the properties of implantable medical devices. Many joints between dissimilar metals, however, suffer from significant intermetallic formation which causes them to fail in a brittle manner. This study investigates a novel process, laser autogenous brazing, being developed by the authors that enables joining of dissimilar metal pairs through a braze-like interface without the use of filler materials to maintain biocompatibility while forming a robust mechanical joint. The formation of brittle intermetallics is mitigated by controlling the thermal profile in the irradiated material through the use of thermal accumulation to limit melting to the joint interface. The strength, composition, microstructure, and fracture surface morphologies of the resultant joints are investigated as a function of processing parameters and thermal simulations are used to aid in understanding the joint formation mechanism.

Introduction

The joining of dissimilar materials is a critical issue in the continued development of advanced medical devices due to the unique properties possessed by materials such as NiTi, Platinum, and Stainless Steel, among others. Requirements for joining of dissimilar biocompatible materials can stem from introducing unique functionalities through the use of shape memory alloys such as NiTi in conjunction with stainless steel (SS), or for decreasing costs while maintaining exceptional corrosion resistance in Pt-to-SS joints. To address these requirements, a new laser joining process is investigated to form autogenous (no filler material) joints between dissimilar, biocompatible metal pairs. The autogenous laser joining process would enable seamless joining of these components and eliminate the need for proprietary adhesives and filler materials used in many current designs.

Laser-based joining processes, due to their low thermal input and small spot size, have become the primary joining mechanism of metallic parts in medical devices such as pacemakers and Implantable Cardioverter Defibrillators (ICDs). The advantages of lasers in joining processes over conventional heat sources, such as minimal heat-affected zones and controlled energy delivery, are vital to medical device manufacturing processes due to the thermal sensitivity of components as well as their continued miniaturization. These same characteristics are crucial in forming reliable joints between dissimilar materials. The tightly controlled heat input allows precise, selective processing and strict control over the melting and intermixing of the two materials.

Of the limited number of metals have been identified as proven or potential biocompatible materials, NiTi and Stainless Steel have received particular attention for use in medical devices. Stainless steel enables physically robust bulk implants and devices with exceptional biocompatibilities at relatively low cost. Smart materials such as shape memory alloys (SMAs) make possible novel device functionalities through thermally-driven actuation and superelastic deformation. The shape memory and superelastic effects of SMAs have been used in medical devices for steerable catheters and stents but are generally limited to monolithic components and suffer from limited radiopacity [1]. Joining different biocompatible material pairs can help to alleviate some of the issues faced by single materials. The ability to form a robust joint between NiTi and stainless steel would enable the incorporation of unique device functionalities (shape memory materials) in low cost medical devices.

Dissimilar metal joints, however, are often complicated by the formation of new phases such as brittle intermetallics within the joint that lead to low strength and premature failure. These phases are typically formed when the two base materials are allowed to mix and result in undesirable mechanical

properties. A number of processes have been investigated for joining dissimilar material pairs that form brittle intermetallic phases. Traditional joining processes have limited spatial selectivity and large heat inputs (arc welding, etc) which promote brittle phase formation. Brazing, which utilizes a filler material with a lower melting temperature than either of the base materials, eliminates melting of the base metals and can potentially avoid intermetallic formation but requires careful selection of the filler material. This is particularly difficult in medical devices due to the required biocompatibility. Li, et al. have investigated the laser brazing of NiTi shape memory alloys to stainless steel using silver-based filler materials but found that the corrosion resistance of the joint was worse than that of the base materials [2].

Solid-state processes can also be performed which allows for greater control over material mixing. One such process, diffusion bonding, has been investigated for direct bonding of biocompatible material pairs such as NiTi/SS by Ghosh and Chatterjee [3], however, the formation of brittle intermetallics could not be prevented. Kundu, et al. [4][5] performed diffusion bonding of the same material pair using Ni and Cu interlayers but also observed the formation of intermetallics at the joint interfaces. In addition, this bonding process requires heating of the entire device to elevated temperatures and, like ultrasonic welding, the ability to impart a compressive stress on the joint. These requirements make such process difficult for medical devices with heat-sensitive components, small size, and complex joint geometries. Intermetallic-free dissimilar metal joints have been achieved through the use of adhesives. These joints, however, are not well suited to extended implantation in the body [6].

In this study, a novel process, autogenous laser brazing, is used to join two biocompatible materials, stainless steel 316L and NiTi. The joint geometry is analysed through optical and scanning electron microscopy (SEM) of sample cross-sections while compositional analysis is performed using energy-dispersive x-ray spectroscopy (EDS). Joint strength is determined though tensile testing to fracture and fracture surface morphology is observed using SEM.

Background

Autogenous Laser Brazing Process

While the majority of laser-based joining processes use the laser input to directly melt the base or filler materials at the joint, the autogenous laser joining process aims to make the joint even smaller than the laser beam spot size. The joining process involves laser irradiation of one of the base materials starting some distance away from and moving toward the dissimilar metal interface. A schematic diagram of the joining process is shown in Figure 1.

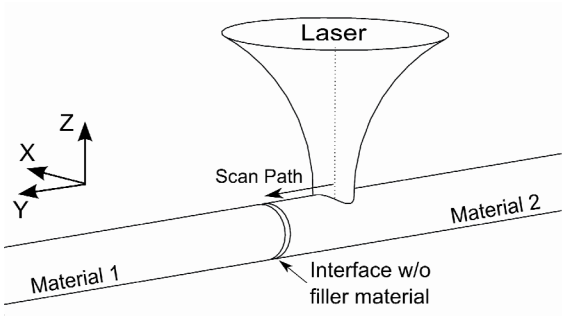

Figure 1: Schematic diagram of proposed autogenous laser brazing process for (a) wire-wire (~400 microns in diameter) Wire-wire process utilizes a Gaussian laser intensity distribution.

Laser parameters such as power and speed are chosen such that the equilibrium temperature of the irradiated piece does not exceed its melting temperature. Heat accumulation due to the thermal resistance of the interface causes the temperature at the interface to rise above the melting temperature of the one of the base materials as the laser beam approaches, forming a molten layer. The laser beam is turned off as the spot reaches the interface and the melt layer is quenched when it comes in contact with the adjacent cold workpiece forming an autogenous braze-like joint.

This process minimizes mixing of the two materials due to the minimal melt volume, high quench rate, and localized melting of one side of the weld joint. This process is also autogenous, eliminating the need for filler materials when joining metallurgically incompatible materials with similar melting temperatures.

Thermal modelling of the joining process is performed using a 3-dimensional finite element code that models half of each of the wires with a symmetric boundary condition on the plane of symmetry to reduce computation time. The laser beam is modelled as a Gaussian beam travelling at a constant velocity across the top of one wire as

$$Q=Q_{max}*\exp(-3/R_o^2*\sqrt{((X-X_o)^2+(Y-(Y_o+Vt))^2)^2}) \quad (1)$$

Where Q is the flux at point (X,Y), Q_{max} is the peak flux, R_o is the beam spot size, X_o and Y_o are the initial position of the laser spot, V is the scan velocity, and t is time. Thermal contact conductance across the dissimilar metal interface is modelled as a step function as a function of temperature with the contact conductance increasing from 1000 for solid-solid

contact to 3000 for solid-liquid contact [7,8]. The contact conductance is spatially resolved over the wire-wire interface allowing for more accurate modelling of the melting phenomenon.

Intermetallic Phases

One of the main impediments to the direct joining of dissimilar metals is the formation of intermetallic phases. These phases are typically highly-ordered and exist within a limited homogeneity range. Due to their highly-ordered and complex structures, many intermetallics have long burgers vectors which limits plastic deformation and renders them extremely brittle. The limited homogeneity range also results in the formation of two-phase microstructures such as dendrites or eutectics unless the composition is within a specific range.

While the formation of intermetallic phases is inevitable in many dissimilar metal pairs at equilibrium, processing techniques have been developed that have shown the ability to decrease intermetallic phase formation or control their microstructures for enhanced strength. Borrisutthekul, et al. [9] have shown that controlling heat flow and cooling rate through increased welding speed and the use of a high thermal conductivity heat sink can decrease the thickness of the intermetallic layer in laser welds between high-strength steel and a 6000-series aluminum alloy. Louzguine, et al. [10] reported the formation of high-strength, high-ductility Ti-Fe bulk alloys which typically form many brittle intermetallics such as TiFe and $TiFe_2$. The results were attributed to the extended solubility of Fe in β-Ti due to the high quench rate as described by Ray [11]. In-situ time and spatially resolved x-ray diffraction methods have been developed by Elmer and Palmer [12][13]and have been used to investigate the formation of phases during welding of Ti-6Al-4V to medium carbon steel dissimilar metal pairs.

Control over the material mixing within dissimilar metal joints has also been investigated for limiting intermetallic phase formation. Borrisutthekul, et al. [14] utilized a specific edge-line lap welding geometry to minimize penetration of the weld pool to the lower plate in laser fusion welding of magnesium and aluminum alloy plates. The effect of interlayers with various compositions for joining Ti and stainless steel was investigated by Lee, et al. [15]. Several studies using laser offsets for composition control of dissimilar metal joints have been reported by Mys and Schmidt [16] and Yao, et al. [17] for copper-aluminum and copper-steel material pairs respectively. The proposed autogenous laser brazing process is designed to minimize mixing of the dissimilar materials as well as increase the cooling rate experienced by the molten material to inhibit intermetallic phase formation while eliminating the need for additional filler materials or adhesives.

Experimental Setup

NiTi and stainless steel 316L wires, roughly 380 and 368μm in diameter, respectively, were cut to 7 inch lengths from spools. One end of each wire was ground flat with the surface perpendicular to the axis of the wire using 800 grit silicon carbide paper. Wires were cleaned in an ultrasonic bath of acetone for 15 minutes prior to assembly in a welding fixture. The welding fixture consisted of a pair of coaxial micro chucks, one holding a stainless steel tube slightly larger than the diameter of the wires. The wire sample to be irradiated by the laser was placed in the tube and allowed to protrude roughly 5mm from the end with the ground end facing the adjacent chuck. The second wire was fixed in the other chuck with its ground end facing the end of the tube. The ground faces of the samples were held together using an axial force applied by a spring on the wire to be irradiated. The axial force on the wires was set to a range between 0.05 and 0.15N by adjusting the compressed length of the spring.

Irradiation along both the stainless steel and NiTi wires was performed using a continuous wave Nd:YAG laser operating at a wavelength of 1064nm. The Gaussian spot was controlled to be the same size as the diameter of the wires. Laser power was adjusted up to a maximum of 4.75W while scan speed and scan distance were adjusted between 0.2 and 1mm/s and 1 and 2.5mm respectively. The laser irradiation was stopped 100μm from the joint interface in order to minimize unnecessary heating of the un-irradiated wire. The sample was allowed to accelerate prior to laser irradiation and decelerate after laser irradiation to ensure that sample translation occurred at a constant velocity during processing. Laser joining was performed in an inert environment of ultra-high purity argon gas which was flowed into the welding fixture at a flow rate of 22cfh.

After joining the samples were tested in tension to fracture using a micro-tensile tester with bollard grips using a cross-head speed of 0.5 mm/min. The gauge length was set at 100mm. Fracture surface analysis was performed using a scanning electron microscope (SEM) while compositional analysis was performed using energy dispersive x-ray spectroscopy (EDS).

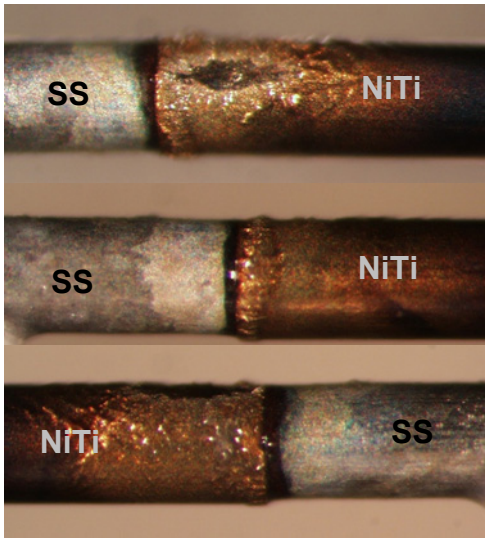

Figure 2: Optical micrograph of dissimilar metal joint between NiTi and Stainless Steel observed from the (a) top and sides (b), (c) of the joint. Sample irradiated on NiTi-side of joint.

Results and Discussion

Weld Geometry

Figure 2 shows a typical joint created using the autogenous laser brazing process. This joint was formed using a laser power of 4.75W directed toward the NiTi wire over a scan length of 2.5mm at a scan speed of 0.5mm/s. Overall, the joint shows a clean outward appearance with no obvious signs of porosity or cracking. A dark spot on the top of the irradiated NiTi wire is observed along with some roughening of its surface, however, no large-scale deformation of the wire is observed indicating that significant melting of the base materials did not occur during processing. Some bulging is observed very close to the joint interface likely due to the softening of the NiTi as it is heated and the axial force applied on the irradiated wire. This deformation indicates that some softening of the material did occur and that the two wires were forced into contact. This is critical for the proposed autogenous laser brazing process since the greater interface conductance caused by the deformation will help to limit the temperature increase at the interface and keep the laser from over melting the wire. In contrast to the irradiated, NiTi, side of the joint, the stainless steel side shows no signs of deformation or surface roughening. This indicates that the temperature on that side of the joint was maintained below the melting temperature.

Figure 3 shows a joint that was formed by irradiating the stainless steel side of the joint. No changes in shape

Figure 3: Optical micrograph of dissimilar metal joint between NiTi and Stainless Steel. Irradiated on SS.

are observed on the irradiated side of the joint while the un-irradiated NiTi wire does show signs of deformation and surface roughening. The deformation being limited to the un-processed side of the joint is likely due to the lower melting temperature of the NiTi compared to the stainless steel. The equilibrium melting temperature of NiTi is 1310°C while for stainless steel it is 1375°C. The irradiated material, with its higher melting temperature, conducts enough heat across the interface to the NiTi for it to melt first and limit further increases in temperature through energy used for the latent heat of fusion and the addition of a new thermal conduction pathway along the un-irradiated wire. The general mechanism of joining is considered to be the same as for the NiTi-irradiated joints with thermal accumulation at the interface limiting melting to the interface.

Figure 4 is an optical micrograph of the same sample shown in Figure 2 after cross-sectioning along the Y-Z plane. A clean interface is observed with little to no porosity, no cracking, and no signs of incomplete joining at the interface. The joint itself is narrowest toward the center of the wires and wider along the top and bottom surfaces. The increased width toward the top of the joint is likely due to the increased heat flux experienced by the top surface from direct laser irradiation which causes excess melting to occur. The bottom of the joint may experience greater melting due to limited heat transfer at the wire surface. Cross-sections performed on SS-irradiated samples show similar joint morphologies (not shown).

Thermal modelling of the autogenous laser brazing process is performed to understand the thermal profile within the wires during irradiation. Figure 5 shows temperature contours in a joint pair with the laser directed at the NiTi wire at a number of different times. Figure 4a shows the steady-state temperature distribution around the laser spot far from the wire-wire interface. Thermal accumulation, as evidenced by the increase in peak temperature, is observed as the laser beam approaches the interface in Fig. 4b and 4c. Some non-uniformity of the temperature at the joint is observed in the thermal model as the laser approaches the interface with the upper region showing a higher temperature consistent with the wider joint observed

experimentally toward the top of the wire. Temperature-time profiles at various distances from the interface are shown in Figure 6. The peak temperature of each point is seen to be a decreasing function of its distance from the joint interface with the faying surface of the joint experiencing the highest temperature rise. This is attributed to the thermal accumulation at the joint due to the imperfect conduction across the interface.

Compositional Analysis

Quantitative EDS profiles performed across the NiTi-SS interface at different depths from the irradiated surface are shown in Figure 7(a-c). Each profile shows a constant composition of primarily Fe in the stainless steel and a slightly Ni-rich composition in the NiTi side of the joint. Between the two base metal compositions is the joined region showing a mixture between Fe, Cr, Ni, and Ti in varying proportions. The extent of this mixed region indicates the width of the joint. The uppermost EDS profile (Fig. 7a) shows a

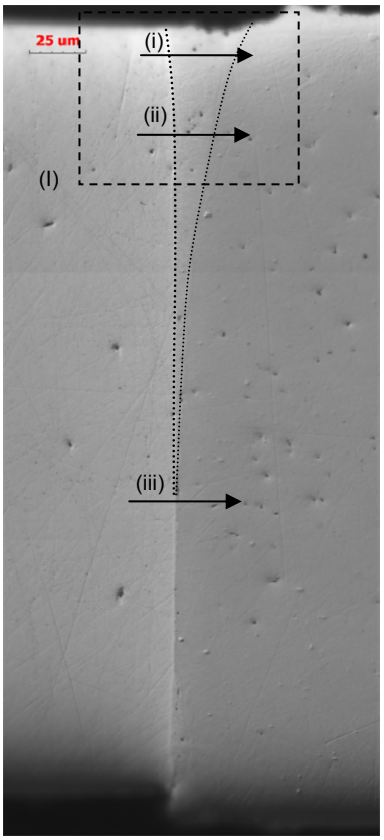

Figure 4: Optical micrograph of joint cross-section. Upper joint region outlined by dotted lines. Note existence of non-zero joint width particularly on top and bottom surfaces of joint.

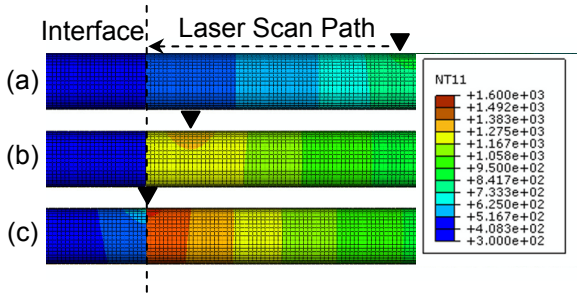

Figure 5: Thermal model of autogenous laser brazing process showing thermal accumulation at joint interface as laser beam approaches. "▼" symbol indicates position of laser beam. (a) Equilibrium temperature distribution far from interface. (b) Beginning of thermal accumulation at interface. (c) Melting of interface.

joint that is roughly 25µm wide. A steep dropoff in the iron and chromium composition, from roughly 75 at% Fe and 20 at% Cr to 10 at% Fe and 3 at% Cr, is observed 25µm from the start of the scan which is the same location at which the Ni and Ti compositions increase significantly, however, an appreciable amount of Fe and Cr are observed to exist roughly 50µm into the EDS line scan. The second EDS profile (Fig. 7b), performed 50µm below the first, shows similar characteristics but with the mixed composition region extending only 15µm from the interface. The third EDS profile (Fig. 7c), performed 175µm below the first does not show a significant mixed region between the two base materials. The entire transition between materials occurs within 5µm at this depth. These different composition profiles suggest that different joining mechanisms are dominant along different regions of the joint. Toward the laser irradiated surface the melted layer thickness is greater, which indicates a

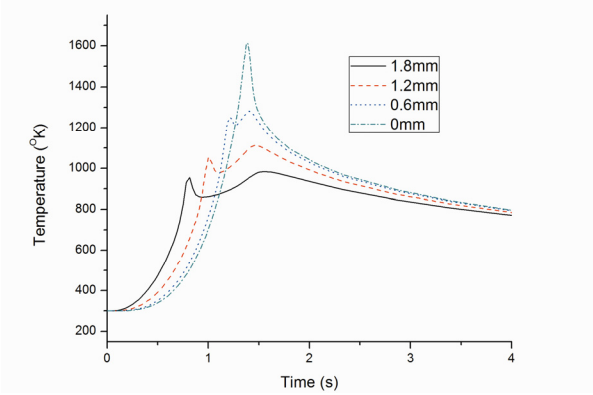

Figure 6: Simulated temperature-time profiles for points at different distances from the joint interface. Note higher peak temperatures for points located closer to the interface indicating thermal accumulation.

longer melt duration, allowing greater dilution of the stainless steel into the molten NiTi. Toward the center of the wires, where minimal mixing of the two materials is observed, the melt layer thickness should be significantly smaller. The composition profile in this region resembles more of a diffusion-controlled process while the upper layers resemble more of a fusion-based joining mechanism. Figure 8 shows an EDS map of region I in Figure 4. A

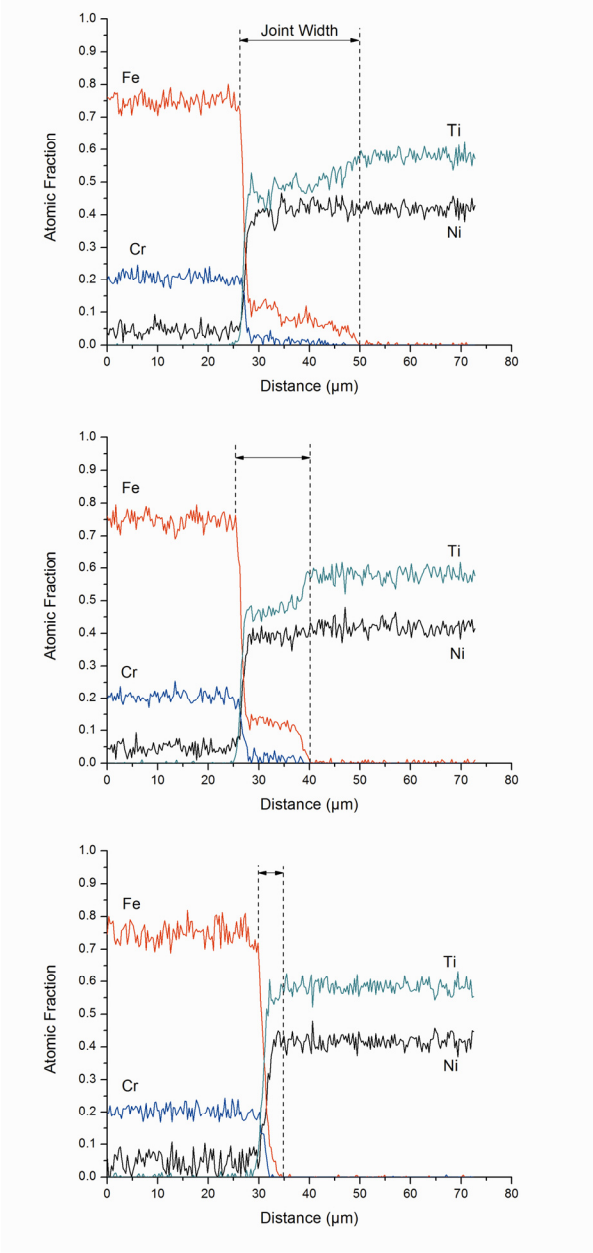

Figure 7: EDX line scan composition profiles for scans (a) i, (b) ii, and (c), iii from Figure 4. Note change in width of mixed zone (joint width) at different locations along wire thickness.

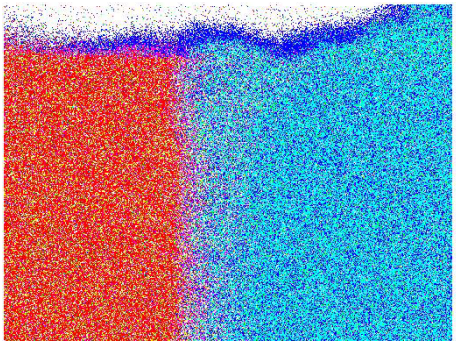

Figure 8: EDS Map of region I in Fig. 4 where red, green, and blue represent Fe, Ni, and Ti.

clear delineation between the two materials is observed with a small layer of mixing between the two. The blue layer on the top of the joint is nearly all Ti and is likely a Titanium oxide. Ti-oxides are expected to form preferentially in these joints due to Titanium's high oxygen affinity.

For samples that were irradiated on the stainless steel side of the joint, similar trends in the joint width and composition profiles are observed. Figure 9 shows the width of the joints at three locations on the joint cross-section as a function of scan speed as determined through EDS line profiles. The joint width can be seen to decrease as a function of scan speed, which is consistent with what was observed for the NiTi-irradiated samples. This is also thought to be due to the decrease in energy put into the wires by the faster laser scan at constant power. At the high end of the scan speed, the joint widths at the top, middle, and bottom of the wire are nearly equal, ranging between 3 and 7μm. The composition profiles for each of these line scans do not show any appreciable mixed zone

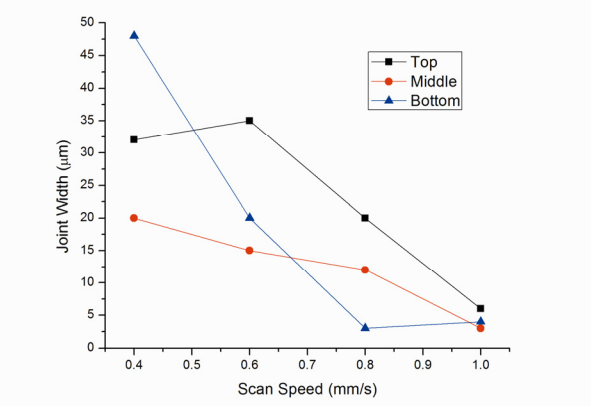

Figure 9: Joint width vs. scan speed for samples processed on the stainless steel side of the joint at constant laser power.

between the base materials as was shown in Fig. 7(c). Thus this joint is expected to be formed primarily though wetting of the SS by the NiTi and some amount of diffusion between the two materials at high temperature. For samples processed at lower speeds with larger joint widths, mixed zones are clearly observed (not shown).

Figure 9 also shows that the joint width is significantly smaller than the beam spot size for all processing conditions. During processing the laser beam is de-focused such that the spot size on the sample surface is roughly 400µm. The largest joint width in Fig. 9 is 48µm while the smallest is only 3µm. Thus the mechanism of joint formation is not direct melting by the laser beam but thermal accumulation as desired.

While the joint width is significantly smaller than the laser beam spot size, it is likely that if the melt pool is able to become large enough or exist for an extended amount of time, convection within the joints may occur due to Marangoni forces resulting in additional mixing and dilution of the base materials. In addition, if the laser scan is performed too slowly, the interface will experience significant pre-heating long before the laser is able to reach the interface and melt the material which will result in unnecessary diffusion between the materials. Due to the axial force exerted on the wires, extended periods at elevated temperatures may also lead to deformation of the base materials and reduction of the contact resistance at the dissimilar metal interface even in the solid state. This would limit the amount of thermal accumulation possible at the interface and may result in incomplete joining.

Figure 10 (a) and (b) show compositional maps over the fracture surfaces of a joint created using the autogenous laser brazing process. The maps for each element have been combined into a RGB color scheme where the intensity of each color represents the signal intensity captured by the EDS for each pixel where red, green, and blue stand for Fe, Ni, and Ti, respectively. Most of the fracture surface, on both the NiTi and SS sides of the joint, are dominated by green and blue which indicates that fracture occurred in Ni and Ti-rich regions of the joint. Quantitative compositional analysis of these regions show that they have a composition of 34.45 at% Ni, 49.46 at% Ti, 12.86 at% Fe, and 3.23 at% Cr on the NiTi fracture surface and 30.43 at% Ni, 44.20 at% Ti, 19.21 at% Fe, and 6.17 at% Cr on the SS fracture surface. Since these compositions are not the same as either base material it can be concluded that fracture is occurring in the joint itself rather than within one of the base materials. Regions with primarily red coloring indicate incomplete joining or fracture in the base SS wire.

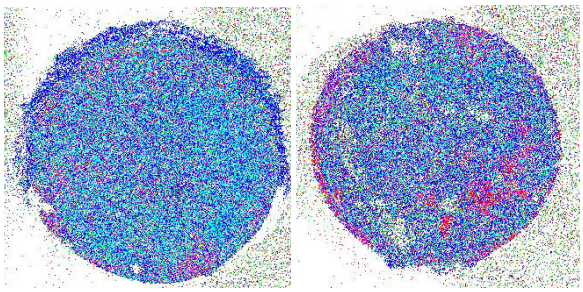

Figure 10: Representative EDS maps of fracture surfaces on (a) NiTi and (b) SS sides of joint. Red, green, and blue, represent Fe, Ni, and Ti.

Joint Strength

An ideal joint between dissimilar materials will have a strength that exceeds the weaker of the base materials. Figure 11 shows the load-displacement curves for the NiTi and Stainless Steel wires in the as-received condition. The stainless steel wire yields at an applied load of roughly 30N and fractures at a load of nearly 60N after significant plastic deformation. The NiTi sample initially deforms elastically until the phase transformation from austenite to martensite occurs at about 50N of applied load. A load plateau is observed at this point as the deformation of the material is accommodated though the phase transformation. After the load plateau another linear elastic region is observed and fracture is observed at nearly 160N of applied load. This load-displacement profile is indicative of the superelastic effect. In a real-world application that requires a joint between these two materials it is likely that the NiTi composition would be adjusted such that the phase transformation occurred before any plastic deformation would be observed in the stainless steel. In the particular NiTi-

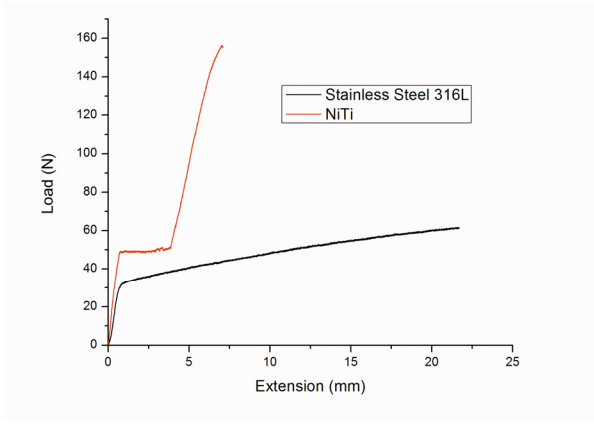

Figure 11: Load-displacement curves for base materials NiTi and Stainless Steel. Note load plateau in NiTi curve indicating phase transformation accommodated deformation (i.e. superelasticity).

SS pair used in this study, the stainless steel will fracture before the NiTi is able to undergo a phase transformation.

NiTi-Irradiated

Each of the composition maps shown in Figure 10 can be further analyzed to determine the uniformity of the fracture surface composition. Figure 12 shows the percentage of the fracture surface area that is dominated by Ni and Ti (<33 at% Fe) along with the joint strength as a function of scan speed. The strength of the joints shows the same qualitative trend as the area fraction values on both sides of the joint with samples showing higher area fractions of Ni and Ti-rich fracture surfaces having higher strengths. Samples that show the same area fractions, however, do not exhibit the same level of tensile strength suggesting that while it has a strong effect the area fraction is not the only determinant of joint strength.

Since the majority of melting will be confined to the NiTi-side of the joint due to its lower melting temperature, any major changes in phase and/or composition are expected to occur toward the NiTi side of the joint. If appreciable amounts of Fe are observed on the fracture surface, a few effects can be considered. First, that there was sufficient mixing of the stainless steel into the NiTi in the solid or liquid phase to increase the atomic fraction in the mixed zone; second, that the joint was strong enough that fracture occurred toward the stainless-steel side of the joint during tensile testing; or, thirdly, for large atomic fractions of Fe on the SS-fracture surface, that there was insufficient melting of the NiTi and that joining was not completed over the entire faying surface.

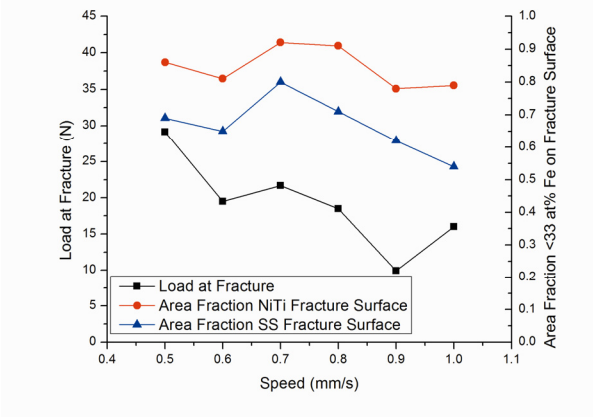

Figure 12: Load at fracture and area fraction of fracture surfaces with <33 at% Fe for samples processed on NiTi-side of joint.

Figure 12 shows a downward trend in the strength with increasing scan speed. As the laser scan speed is increased the overall energy input into the wire is reduced. As discussed above, this can have the effect of decreasing the melt layer thickness or eliminating the melt layer all together. As the scan speed increases the area fraction that is NiTi dominated remains high on the NiTi fracture surface but decreases on the SS fracture surface. Decreases in NiTi-dominated regions suggest that some areas experienced incomplete joining. As scan speed is increased, the uniformity of temperature at the interface is reduced which can result in insufficient melting to cover the entire faying surfaces resulting in decreased strength.

SS-Irradiated

Figure 13 shows the load at fracture achieved during tensile testing of samples irradiated on the stainless steel side of the joint as a function of scanning speed along with the area fraction of the NiTi fracture surface with <33at% Fe. A higher area fraction suggests that there is less dilution of Fe into the NiTi. The two curves in Figure 13 show opposite qualitative trends with the load at fracture being lower for higher area fractions. In addition, unlike the NiTi irradiated samples shown in Figure 12, the strength is highest for the highest scan speed. Since the strength is seen to decrease for higher area fractions with significant Fe on the NiTi side, the decrease in strength is likely due to melting of the stainless steel during processing. Since laser irradiation is occurring on the SS-side of the joint, it is possible that some melting is occurring on the SS-wire surface causing enhanced dilution of the materials. This causes greater mixing to occur at the interface between the two molten base materials, causing brittle intermetallic phases to form, decreasing the strength of the joints.

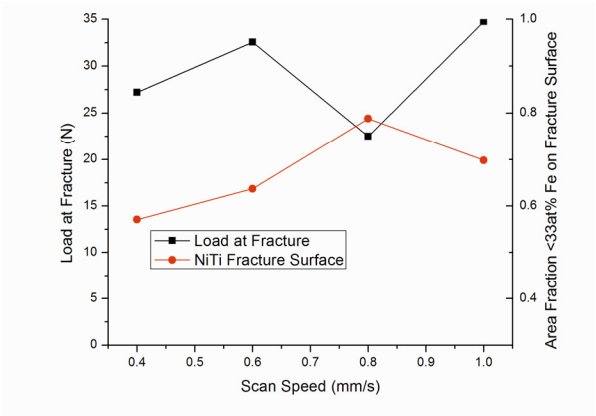

Figure 13: Load at fracture and area fraction of fracture surface with <33 at% Fe for samples processed on SS.

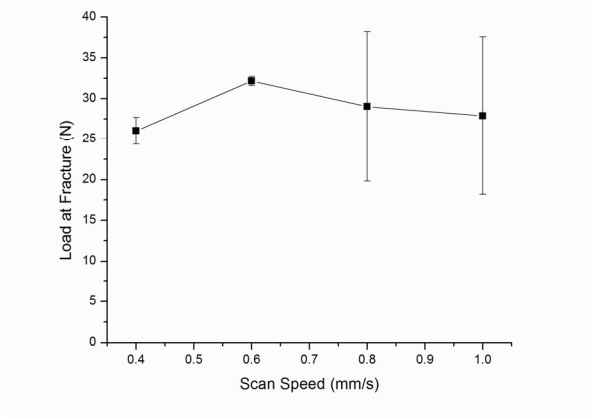

Figure 14: Load at fracture with standard deviation for samples processed on SS-side. Note greater variability in joint strength at higher scan speeds.

Figure 14 shows the average strength for samples irradiated on the stainless steel side as a function of scan speed along with the standard deviation. While the number of data points for these particular parameters is limited, it was observed that, in general, the joints produced at higher speeds have higher maximum loads at fracture but greater variability while the joints produced at slower speeds are not as strong but more consistent. This variability in joint strength for higher scan speeds suggests that the amount heat accumulation and melting is highly sensitive to joint

parameters when limited thermal energy is input into the system. The thermal contact between the two faying surfaces of the joint is considered to be one of the main controlling variables in this case. While the two wires are fixtured and ground flat to provide consistent mating surfaces, the perpendicularity of the face to the axis of the wire cannot be precisely maintained. This causes the two faces to be misaligned which significantly alters the thermal contact resistance across the dissimilar metal interface before processing, a critical parameter for achieving a consistent and thin melt layer at the interface. At the lower scan speeds, even when there is good contact across the interface, the laser is inputting enough energy into the wire to form a melt layer. If the contact is not good, the slow laser scan overheats the wire causing a thicker melt layer to form. At higher scan speeds, good thermal contact results in no melt layer at all while lower thermal conductance leads to very thin melt layers which is expected to be the ideal melt geometry. Thus, greater control over the geometry and alignment is required to create dissimilar joints with strengths greater than the base materials.

Fracture Surface Analysis

The load-displacement curves for the two base materials shown in Figure 11, above, along with electron micrographs of the associated fracture surfaces (not shown), confirms that the base materials fail through ductile fracture. While some of the joints produced using the new autogenous laser joining process have reached strengths close to the yield strength of the stainless steel, no significant ductility has been observed during tensile testing. Figure 15 shows a typical fracture surface as seen through electron microscopy for a sample joined using the autogenous laser joining process. The surface has a morphology indicative of quasi-cleavage fracture, and as discussed above, fracture is believe to be occurring within the joint, not in the base material. While some plastic deformation is believe to be occurring at the joint, the overall fracture mechanism is still primarily brittle.

Conclusion

A new joining process, laser autogenous brazing, has been investigated for creating seamless joints between two biocompatible materials, NiTi and Stainless Steel 316L for medical device applications. The joints show strengths which approach the yield stress of the stainless steel base material during tensile testing and have fracture surfaces indicative of quasi-cleavage fracture. EDS mapping of the cross-sections indicated that joint widths were significantly smaller than the incident laser beam diameter while fracture surface maps suggested that joint strength is closely tied to compositional uniformity and complete joining of the observed, the joint strengths achieved suggest that laser autogenous brazing is a viable and promising method for creating robust joints between the NiTi and Stainless Steel biocompatible dissimilar material pair.

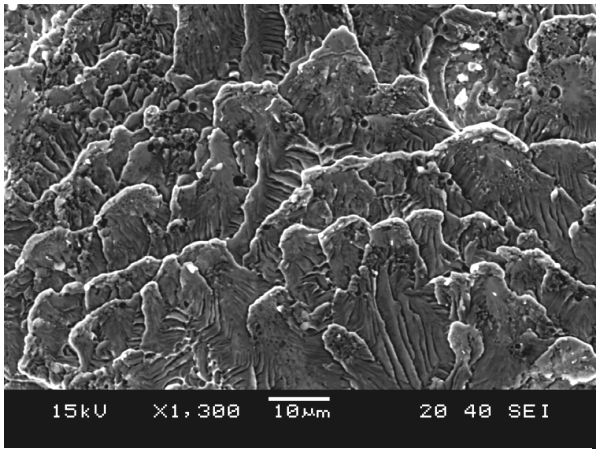

Figure 15: SEM of fracture surface for sample irradiated on SS suggesting quasi-cleavage fracture.

References

[1] Hilfiker P. R., Quick H. H., Schmidt M., Debatin J. F. (1999) In vitro image characteristics of an abdominal aortic stent graft: CTA versus 3D MRA., *Magma (New York, N.Y.)*, **8**, pp. 27-32.

[2] Li M. G., Sun D. Q., Qiu X. M., Yin S. Q. (2006) Corrosion behavior of the laser-brazed joint of TiNi shape memory alloy and stainless steel in artificial saliva, *Materials Science and Engineering A*, **441**, pp. 271-277.

[3] Ghosh M., Chatterjee S. (2002) Characterization of transition joints of commercially pure titanium to 304 stainless steel, *Materials Characterization*, **48**, pp. 393-399.

[4] Kundu S., Ghosh M., Laik a, Bhanumurthy K., Kale G., Chatterjee S. (2005) Diffusion bonding of commercially pure titanium to 304 stainless steel using copper interlayer, *Materials Science and Engineering: A*, **407**, pp. 154-160.

[5] Kundu S., Chatterjee S. (2008) Characterization of diffusion bonded joint between titanium and 304 stainless steel using a Ni interlayer, *Materials Characterization*, **59**, pp. 631-637.

[6] Bauer I., Russek U. A., Herfurth H. J., Witte R., Heinemann S., Newaz G., Mian A., Georgiev D., Auner G. W. (2004) Laser microjoining of dissimilar and biocompatible materials, *Proceedings of SPIE*, pp. 454-464.

[7] Mesnyankin S. Y., Vikulov A. G., Vikulov D. G. (2009) Solid-solid thermal contact problems: current understanding, *Physics-Uspekhi*, **52**, pp. 891-914.

[8] Goudie N., Argyropoulos S. (1995) Technique for the estimation of thermal resistance at solid metal interfaces formed during solidification and melting, *Canadian Metallurgical Quarterly*, **34**, pp. 73-84.

[9] Borrisutthekul R., Yachi T., Miyashita Y., Mutoh Y. (2007) Suppression of intermetallic reaction layer formation by controlling heat flow in dissimilar joining of steel and aluminum alloy, *Materials Science and Engineering A*, **467**, pp. 108-113.

[10] Louzguine D. V., Kato H., Louzguina L. V., Inoue A. (2004) High-strength binary Ti-Fe bulk alloys with enhanced ductility, *Journal of Materials Research*, **19**, pp. 3600-3606.

[11] Ray R. (1972) The constitution of metastable titanium-rich Ti-Fe alloys:An order-disorder transition, *Metallurgical Transactions*, **126**, pp. 362-629.

[12] Elmer J. W., Palmer T. A., Babu S. S., Zhang W., DebRoy T. (2004) Phase transformation dynamics during welding of Ti – 6Al – 4V, *Journal of Applied Physics*, **95**.

[13] Elmer J. W., Palmer T. A. (2006) In-situ phase mapping and direct observations of phase transformations during arc welding of 1045 steel, *Metallurgical and Materials Transactions A*, **37A**, pp. 2171-2182.

[14] Borrisutthekul R., Miyashita Y., Mutoh Y. (2005) Dissimilar material laser welding between magnesium alloy AZ31B and aluminum alloy A5052-O, *Science and Technology of Advanced Materials*, **199**.

[15] Lee M. K., Lee J. G., Choi Y. H., Kim D. W., Rhee C. K., Lee Y. B., Hong S. J. (2010) Interlayer engineering for dissimilar bonding of titanium to stainless steel, *Materials Letters*, **64**, pp. 1105-1108.

[16] Mys I., Schmidt M. (2006) Laser Micro Welding of Copper and Aluminum, *Proceedings of SPIE*, pp. 610703-1-6.

[17] Yao C., Xu B., Zhang X., Huang J., Fu J., Wu Y. (2009) Interface microstructure and mechanical properties of laser welding copper–steel dissimilar joint, *Optics and Lasers in Engineering*, **47**, pp. 807-814.

Meet the Authors

Gen Satoh received his B.S. from Harvey Mudd College and his M.S. from Columbia University. He is currently a doctoral student at the Manufacturing Research Laboratory at Columbia University.

Dr. Y. Lawrence Yao is currently a professor of Columbia University's Mechanical Engineering Department and director of the Manufacturing Research Laboratory. He received his Ph.D. from the University of Wisconsin-Madison in 1988.